Chapter 11
High-Pressure Hydrogenated Carbon Nanostructures*

[AU1] **A.V. Bazhenov[1], I.O. Bashkin[1], and K.P. Meletov[1]**

Abstract High-pressure hydrogenation of the single-walled carbon nanotubes, graphite nanofibers and fullerenes C_{60} was developed. Produced samples have been studied by their combustion, gas thermodesorption, mass-spectroscopy, X-ray, IR and Raman scattering spectroscopes.

Synthesized carbon nanotubes, graphite nanofibers with the hydrogen content corresponding to the chemical formula $CH_{0,8\div0,9}$ and fullerenes $C_{60}H_x$ with x from x = 36 to the unbelievable x = 60 were produced and elucidated. Physisorption takes place only for small percent of hydrogen in this case. Dominant amount of hydrogen forms the strong covalent C–H bonds thermally stable up to 600°C. As a result of hydrogenation high-frequency conductivity of free carriers in nanotubes decreases by one order of magnitude and electron transitions between van Hove singularities in the density of electron states of nanotubes disappear.

We have shown that $C_{60}H_{36}$ is a set of isomers in our case. Combination of the vibrational modes of $C_{60}H_{60}$ and, for example, $C_{60}H_{48}$ can explain the emission and absorption spectra of interstellar and circumstellar clouds: spectral positions of not only narrow lines, but broad backgrounds as well.

Hydrogen interaction with the carbon nanostructural materials (nanotubes, nanofibers, fullerenes C_{60} and C_{70} has been intensively studied over the last years. A developed surface of nanotubes and nanofibers induced a considerable applied interest aimed at hydrogen storage and reduced consumption of organic fuel in modern industry. For the academic studies, of interest is the nature of the hydrogen interaction with the carbon nanomaterials.

In view of practical application, the carbon nanotubes or nanofibers were saturated with molecular hydrogen under relatively mild conditions: the hydrogen

[1]Institute of Solid State Physics, Chernogolovka, Moscow District, Russia
e-mail: bazhenov@issp.ac.ru

*In *Medicinal Chemistry and Pharmacological Potential of Fullerences and Carbon Nanotubes*, Franco Cataldo and Tatiana Da Ros (eds.), Springer Vol. 1, Topics in Carbon Materials: Chemistry and Physics, 2007

F. Cataldo and S.Iglesias-Groth (eds.), *Fulleranes: The Hydrogenated Fullerenes*, Carbon Materials: Chemistry and Physics 2, DOI 10.1007/978-1-4020-9887-1_11,

pressure did not exceed 10 ÷ 12 MPa at room or liquid nitrogen temperatures. The data of the application research were reviewed, e.g., by Dillon and Heben (2001). The processes of hydrogen absorption and desorption in the compression/decompression cycles were found to be reversible and reproducible at any temperature. It was generally assumed on the basis of the absorption/desorption data, that the mechanism of the hydrogen absorption is physisorption of the H_2 molecules on the graphene layers The data on the electrical properties and Raman spectra of the single-walled nanotubes measured in the hydrogen absorption/desorption cycles at pressures up to 0.8 MPa and temperatures from 4 to 500 K (Pradhan et al. 2002) supported the assumption of hydrogen physisorption. There was, however, a remarkable discrepancy as concerns the hydrogen capacity: the maximal amount of absorbed hydrogen reported by different authors showed a scatter by two orders of magnitude, from several tenths to several tens of wt% H. Numerous studies have shown that maximum amount of adsorbed hydrogen is ≈6 wt% H.

An alternate approach was the study of hydrogen chemical reaction with fullerenes producing strong chemical bonds. There were some works on interstitial solution of molecular hydrogen in fullerenes (e.g., Assink et al. 1992), but the main efforts were made to their chemical modification. There have been proposed several hydrogenation reactions where fullerenes C_{60} or C_{70} acted as traps of hydrogen (discussed in many reviews, e.g., Taylor and Walton 1993; Hirsch 1994; Goldshleger et al. 1997). [AU2] [AU3]

Fullerenes could be hydrogenated in organic solvents due to the metal-acid reaction, or due to the hydrogen transfer from a hydrogen-rich compound like 9,10-dihydroanthracene, or in the presence of hydrogenation catalysts and so on. Hydrogen binding in the reaction products was stronger compared to physisorption because of formation of the strong covalent C–H bonds. There were prepared many compounds $C_{60}H_x$ and $C_{70}H_x$ with even values of x. The most complete study of the properties was carried out on $C_{60}H_{\sim 36}$ and $C_{60}H_{18}$. Maximal content of hydrogen was x = 36. We know only one publication where more hydrogen-rich compounds with x = 38–50 have also been observed in the mass spectra of the products of catalytic hydrogenation (Shigematsu et al. 1993).

Direct fullerene hydrogenation was accomplished at hydrogen pressures elevated to 50–85 MPa and T = 573–623 K (Jin et al. 1994). Later this method was widely used to prepare hydrofullerenes of the some compositions as after the chemical reactions. The chemical potential of hydrogen increases under pressure, and there are many examples of the increase in hydrogen solubility or the formation of hydride phases in the metal–hydrogen systems at high pressures. The technique used in our work provides hydrogen pressures up to 9 GPa at temperatures from 77 to 900 K. With these treatment parameters, it was possible to prepare new hydrogen-rich compounds on the basis of the carbon nanomaterials with covalently bound hydrogen.

High hydrogen pressures were generated using the toroid-type quasi-hydrostatic devices. A general view of the high-pressure cell is shown in Fig. 11.1. A sample of about 100 mg mass and a pellet of AlH_3 (or AlD_3) were placed into a copper ampoule and separated with a thin Pd foil. The ampoule was tightly plugged with

BookID 185609_ChapID 11_Proof# 1 - 27/01/2010

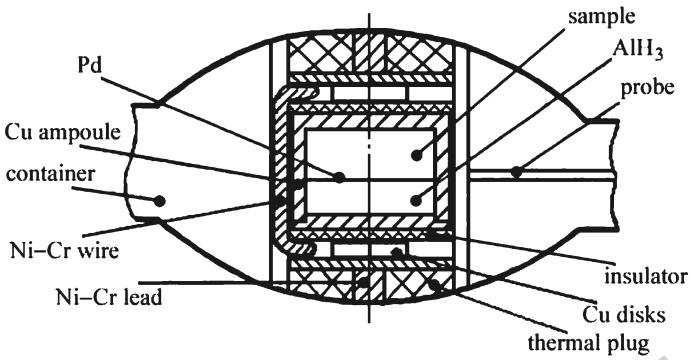

Fig. 11.1 Layout of the high-pressure cell

a copper lid using gallium as solder. Both Cu and Ga are less permeable to hydrogen and retain it in the ampoule. Thermally unstable AlH_3 rapidly decomposed under high pressure on heating above 250°C, permeated through the Pd foil and reacted with the sample. The ampoule was mounted in the channel of a pipestone container together with the Ni–Cr wire heater, a thermocouple entered through a special probe hole. The container also served as a pressure-transmitting medium.

The procedure of the thermobaric treatment consisted of several steps. Initial compression to 1.5 GPa and heating to 270°C resulted in the hydrogen atmosphere in the ampoule. Then pressure was increased to the final value, and the sample was maintained at 350°C overnight (about 20 h), then at 450–490°C for 6–10 h. After cooling to room or liquid-nitrogen temperature and decompression, the recovered samples were stored without access of the ambient atmosphere until measurements.

11.1 Experimental Methods for Testing of Samples

The chemical analysis of the products was carried out using combustion of a 3 mg sample in the oxygen flow at 1,100°C and weighting of the combustion products, CO_2 and H_2O (or D_2O).

The X-ray diffraction patterns were measured at room temperature on a Siemens D500 diffractometer with the monochrome $CuK_{\alpha 1}$ irradiation.

The thermal stability of the hydrogenated materials was estimated by measurements of gas thermodesorption. A piece the sample cooled to liquid nitrogen under pressure was placed, in a liquid nitrogen bath, into a non-hermetic copper container, and the latter was moved into a quartz ampoule externally cooled with liquid nitrogen. The ampoule was connected to a vacuum system with the calibrated volume, the system was evacuated to 10^{-6} MPa, and then the ampoule was heated at a rate of 20 K/min. The pressure P of a gas evolved upon heating to 650°C was registered manually; the sample was weighed after measurements. We call these dependences as a "manometric curves".

The mass spectra of the gases evolved from the deuterated SWNT sample heated in vacuum were measured with the MI 1201V mass spectrometer. Gas ionization in the ion source of the spectrometer was produced with a 70-eV electron beam. To obtain the gas phase, the sample was placed in a quartz ampoule of a pyrolyzer that was connected to the injection system of the mass spectrometer through a fine control valve. Then the ampoule was evacuated to a pressure of about $2\cdot\times 10^{-5}$ Pa in order to remove the surface and weakly bound impurities from the sample. After the evacuation, the ampoule was isolated from the vacuum system and the sample was heated to 550°C in five steps. At each step, the sample was kept at a fixed temperature for 3 h; then the fine control valve was open and the mass-spectrometric analysis of the gas collected in the ampoule was performed. After the analysis, the quartz ampoule was again evacuated, the valve was closed, and the sample was heated to the next temperature. The measurements were carried out over the range $1 \le m/z \le 90$, where m is the atomic mass and z is the ion charge. The spectrometer resolution of about 0.08% ensured a reliable determination of the gas-phase components.

IR spectra were measured by Bruker IFS-113v IR Fourier spectrometer: transition spectra and diffuse reflection at T = 295 K. IR microscope of the Fourier spectrometer was used for the measurements of the transmission spectra in the spectral range 600–9,000 cm^{-1} Transmission spectra of the thin films were also measured in the spectral range from 4,000 to 18,000 cm^{-1} using a standard double-beam spectrometer.

Raman spectroscopy: Raman spectra from small SWNT pieces with typical dimensions of 100 μm were recorded in the back-scattering geometry using two different micro-Raman setups comprised of a triple monochromator DILOR XY and a CCD detector system, cooled either to liquid nitrogen temperature or −100°C. The 488 or 514.5 nm line of an Ar^+ laser, as well as the 647.1 nm line of a Kr^+ laser, were used for excitation, while the beam intensity on the sample was ≅0.5 mW. The laser line was focused on the sample by means of a 100× objective with a spatial resolution of ~1 μm.

11.2 High-Pressure Hydrogenated Single-Walled Carbon Nanotubes and Nanofibers

Our first results about the high-pressure hydrogenation of single-walled carbon nanotubes (SWNTs) and graphite nanofibers (GNFs) were published in (Bashkin et al. 2004). Starting GNFs were synthesized in a direct-flow quartz reactor in a CO/H_2 = 4/1 gas mixture at 600°C for 6 h using a mixed Fe/Cu = 7/3 catalyst. Scanning electron microscopy showed that the GNF length was, on the average, of 30 μm and the diameter ranged from 100 to 300 nm. The content of graphite nanofiber in the prepared material was about 90%.

Carbon black containing 15–20% SWNTs was synthesized by the electric arc method in helium atmosphere at a pressure of 0.86 atm using a metallic Co/Ni = 3/1 catalyst (Loutfy et al. 1999). To remove impurities from SWNTs, carbon black

was subjected to ultrasonic treatment in a concentrated hydrochloric acid, and then to the multistage treatment with hydrochloric acid alternating with oxidation in air at temperatures up to 540°C. The content of SWNTs in the product was estimated using scanning and transmission electron microscopy and was found to be equal to 50–60%.

In the experiments, a GNF or SWNT sample with a mass of about 60 mg was placed in a high-pressure chamber and saturated with hydrogen obtained by thermal decomposition of AlH_3. The sample was held under a hydrogen pressure of 9 GPa first for 18 h at t = 350°C and then for another 6 h at 450°C. At the end of holding, the chamber was cooled to −140°C and unloaded to atmospheric pressure at this temperature. Then, the hydrogen-saturated material was taken out from the chamber and further held in liquid nitrogen.

Hydrogenated GNF and SWNT powders with a mass of several milligrams were chosen to determine their thermal stability, hydrogen content and to study them by X-ray diffraction, IR spectroscopy and so on.

The typical manometric curves for hydrogenated GNFs and SWNTs are shown in Fig. 11.2. The right axis of the graph indicates the amount of liberated hydrogen x as calculated under the assumption that the gas consisted only of H_2 molecules. The x(t) dependences for hydrogenated GNFs and SWNTs are closely similar to each other. In the interval from T = 77 K to t = 0°C, the amount of liberated gas increases with temperature rather slowly, a small jump is observed near t = 0°C, and the gas release is terminated near room temperature. The total amount of hydrogen released upon heating to room temperature is 0.15–0.5 wt%. Gas is virtually not evolved from the samples upon heating from room temperature to 450°C, but the second stage of intense release begins near 600°C, and about 5 wt% H is collected at 600–650°C, i.e., an order of magnitude greater than upon heating to room temperature. The rate of gas release is low, so that the process is not terminated up to 600–650°C, and, as is shown in Fig. 11.2 by the example of GNF–H_x, an additional amount of gas is liberated upon repeated sample heating to 600°C at the same rate.

To determine the total hydrogen content and estimate the composition of liberated gas, the hydrogenated GNF and SWNT samples heated to room temperature were burned out in an oxygen flow at 1,400°C and the combustion products H_2O and CO_2 were weighed. These measurements gave x = 6.3 wt% H for GNF and x = 6.8 wt% H for SWNTs (this corresponds to the chemical formulas $CH_{0.81}$ and $CH_{0.88}$, respectively), with a spread in data less than 0.05 wt%. The data obtained agree satisfactorily with the estimate $x \approx 5$ wt%H derived from the gas release between room temperature and 650°C, taking into account that the gas release was incomplete during the first run. Such an agreement is the evidence that hydrogen was liberated predominantly in the form of H_2 molecules rather than of hydrocarbons (e.g., if methane CH_4 were released, the amount of its molecules and, correspondingly, pressure would be twice as low in the gas-release experiments). A comparison of the burning results with the gas-release data allows the conclusion to be drawn that, after measurements with heating to 600–650°C presented in Fig. 11.2, about 1.2 and 1.7 wt% H remained in the GNF and SWNT samples, respectively.

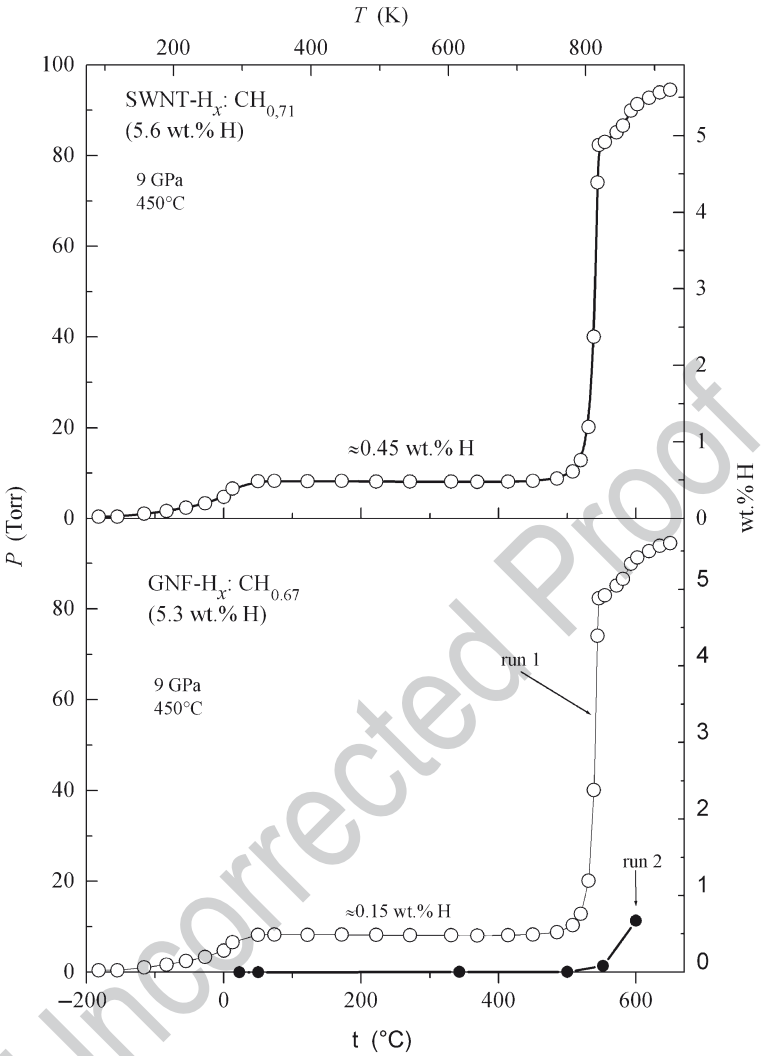

Fig. 11.2 Temperature dependence of the gas pressure in a preliminarily evacuated volume (*left vertical scale*) and its recalculation into the amount of hydrogen evolved from the sample (*right scale*) upon heating at a rate of 20 K/min for single-walled carbon nanotubes (SWNTs) and graphite nanofibers (GNFs, two heating cycles) saturated with hydrogen at a pressure of 9 GPa and temperatures up to 450°C

Mass-spectrometer date of the hydrogenated carbon nanotubes we have published in (Shulga et al. 2004). These nanotubes for the gas mass-spectrometry were synthesized by the electric-arc method using a nickel–yttrium catalyst. To remove amorphous carbon and the metal catalyst, the primary products containing 10–15 wt% of carbon SWNTs were purified by repeated oxidation in air at temperatures

up to 550°C alternated with washing in hydrochloric acid. The microprobe analysis showed that final content of the metal impurities in SWNT was less than 1 wt%, with the ratio of the detected metals Ni:Y:Cu:Zn = 1:1.5:0.6:0.7. The incombustible residue was consistent with the total oxide amount within ±30%. The purified products were studied using the high-resolution electron microscopy (Krestinin et al. 2003a, b). The sensitivity of the absorption spectra in the near-IR region to the purity of products (Krestinin. et al. 2003; Chiang et al. 2001) was used for quantitative determination of the SWNT content in this batch, it amounted to 80–85 wt%. The nanotubes had a narrow diameter distribution with an average value of 1.5 nm and were strongly aggregated in bundles, microcrystalline films, and polycrystalline covers. The main carbon impurities, according to the electron-microscopic data, were graphitized black particles and graphite blocks up to 10–15 μm in size.

To reduce or to take into account the effect of the ambient atmosphere and other experimental factors, we used the heavier hydrogen isotope, deuterium, in this study. SWNTs deuterated under the final pressure of 5 GPa during a two-step exposure at T = 350°C for 21 h and at T = 460–490°C for 9 h. According to the data of two combustion tests, deuterated SWNT contained 10.8 ± 0.1 wt% D.

The mass spectra of gases evolved from deuterated SWNT at various heating steps are shown in Fig. 11.3. The main constituent of the gas phase at temperatures to 400°C was a mixture of the hydrocarbon molecules and radicals. The mixture consisted of both deuterated hydrocarbons, as evidenced by the high intensities of the peaks with m/z = 17–20 and 31–36, and compounds including the light isotope, as follows from the occurrence of the peaks with the odd mass numbers. The latter fact is indicative of the impurity of the light hydrogen isotope, protium. The occurrence of a minor impurity of protium both in parent SWNT and in AlD_3 was found in other experiments. The origin of protium in AlD_3 is quite clear: our AlD_3 contains approximately 8% admixture of the AlH_3. Parent SWNT had a minor impurity of solvents and media used for their preparation, diethyl ether and acetone, whose fragmentation products were ascertained by the analysis of the fine structure of the peaks at m/z = 28, 31, 44, 45, 59, and 74 (Shulga et al. 2004).

The most prominent feature of the spectra in Fig. 11.3 is a dramatic difference between the compositions of the gas phase below and above 400°C. The concentration of the D_2 molecules in the gas phase increased as the temperature was increased from 100°C to 400°C. In the spectra measured after heating to 500°C and 550°C, the peaks with m/z = 4 and 3 became dominant. Consequently, D_2 and HD molecules were the main components of the gas phase at these temperatures. This remarkable fact shows that the main step in the manometric curves in Fig. 11.3 is actually due to evolution of molecular hydrogen whereas light hydrocarbon molecules contribute mainly at lower temperatures when the gas desorption is small.

Figure 11.4 shows the X-ray diffraction patterns of GNFs and SWNTs in the initial and hydrogenated states and after various annealing procedures. Partial annealing with the removal of ≈40% of hydrogen absorbed under pressure

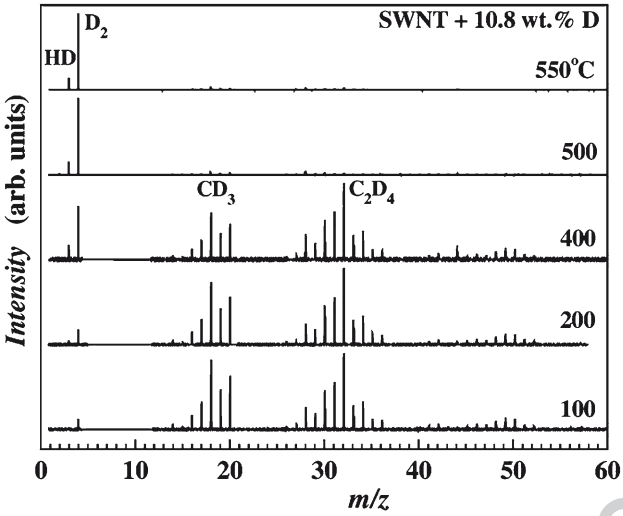

Fig. 11.3 Mass spectra of the gas phase over a sample of deuterated SWNT measured in heating steps at indicated temperatures. The spectra are restricted to the m/z = 60 value, because peaks of the heavier ions have negligible intensities. The most intense peaks are identified according to their principal components

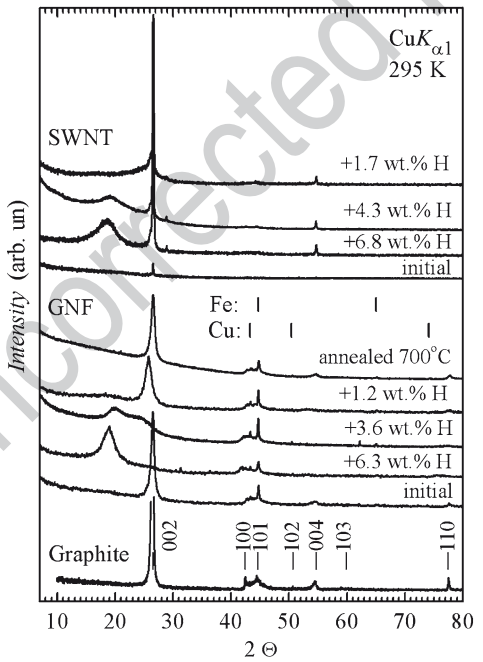

Fig. 11.4 X-ray diffraction patterns of single-walled carbon nanotubes and graphite nanofibers: in the initial state, after saturation with hydrogen at 9 GPa (6.8 and 6.3 wt% H, respectively), after removal of about 40% of absorbed hydrogen (4.3 and 3.6 wt% H), after degassing annealing at 600–650°C (1.7 and 1.2 wt% H), and after prolonged annealing at 700°C (GNFs). For comparison, the diffraction pattern of a GDG-6 graphite powder is also shown. Bar diagrams of Fe and Cu indicate the catalyst admixture in GNFs, T = 295 K

BookID 185609_ChapID 11_Proof# 1 - 27/01/2010

(the residual contents were 3.6 wt% H in GNFs and 4.3 wt% H in SWNTs) was carried out by holding the sample in an evacuated volume at a temperature of about 500°C. Annealing of GNFs at 700°C was performed in a dynamic vacuum of $P < 10^{-5}$ mmHg for 6 h. The X-ray diffraction pattern of the ground high-density graphite GDG-6 is presented in Fig. 11.3 for comparison.

The diffraction patterns of initial GNFs include a strong reflection near the graphite (002) line at $2\Theta = 26.5°$, a number of weak reflections near the other graphite lines, and the lines of catalyst components. After the saturation of the GNFs with hydrogen, a broad intense peak appears near 19° instead of a very strong graphite reflection at $2\Theta = 26.5°$, the other graphite reflections undergo a marked shift to the small angles, and only the catalyst lines do not change their positions. After two heating cycles to 600°C shown in Fig. 11.2, the peak at 19° disappears and the diffraction pattern mainly regains its initial shape. Nevertheless, the most intense reflection remains markedly shifted to small angles, in agreement with the fact that hydrogen is removed incompletely. A prolonged vacuum annealing at 700°C results in a complete recovery of the initial diffraction pattern. A comparison of the diffraction pattern of the sample having 3.6 wt% H after partial annealing with the diffraction patterns of the extreme states shows that it represents the diffraction pattern of a two-phase state, in which the strongest reflections are shifted toward each other ($2\Theta \approx 19.9°$ and 24.0°) and are strongly broadened. A change in the X-ray diffraction patterns indicates that the crystal lattice of graphite nanofibers swells upon hydrogenation and that the structure is recovered after the removal of hydrogen.

In the diffraction pattern of the initial SWNTs, no reflections are seen from the single-walled nanotubes (a weak reflection at small angles $2\Theta \sim 6°$ can be, in principle, observed because of the triangular SWNTs packing in bundles (see e.g. Sharma et al. 2001). A sharp weak reflection at the position of the graphite (002) line should be caused by the presence of an admixture of graphitized particles in the material. The catalyst reflections are not seen. After the hydrogenation of the SWNTs, a broad peak appears near 18.5°. A change in the diffraction pattern of the multilayer GNF structure upon hydrogenation, 6.3 wt% H, can be considered as being caused mainly by an increase in the spacing between the graphene layers by approximately 40% from 3.36 to 4.67 Å. The narrow graphite (002) and (004) reflections are markedly strengthened. We think that it is just the result of the crystallization of the amorphous graphite micro inclusions. The removal of 2.5 wt% H results in weakening of the broad peak 18.5° and its shifting by ≈0.8° to larger angles, and this peak disappears after heating to 650°C. The sharp graphite (002) and (004) reflections are retained and their intensity relative to the background change only slightly. It was reported in the literature that SWNT is not destroyed at hydrostatic pressures below 13 GPa (Sharma et al. 2001). For this reason, a change in the diffraction pattern of SWNTs after the thermal treatment in hydrogen should be assigned to the graphitization of the amorphous carbon particles that are the impurity addictions in the initial material and to the hydrogenation and dehydrogenation of a certain fraction of graphitized particles.

Weakly bonded hydrogen, which is released in an amount of less than 0.5 wt% upon heating to room temperature, can reasonably be assigned to physisorption, which is considered to be the dominant mechanism of hydrogen absorption by carbon materials at pressures below 12 MPa and not too high temperatures.

To elucidate the nature of the bonded states of the main hydrogen mass that is retained up to high temperatures, the IR diffuse reflection spectra were measured for GNF and SWNT powders in the initial state, after the treatment under hydrogen pressure, and after the degassing annealing. Measurements were performed in the range 400–5,000 cm^{-1} at room temperature. The results are presented in Fig. 11.5.

It is not the conventional reflection but the diffuse reflection of powder. Light in this sample is scattered over 2π solid angle. The spectra of initial GNFs and SWNTs (curves 1 of Fig. 11.5) are characterized by a monotonic decrease in intensity with the increase of the photon energy; such a spectral behavior is typical of the spectra of purified nanotubes (Bazhenov et al. 1998). As in the case of nanotubes exhibiting properties of a strongly imperfect metal or semimetal, the light absorption by free carriers caused by their high-frequency conductivity is the main reason for a decrease in the GNFs and SWNTs diffused reflection with increasing photon energy.

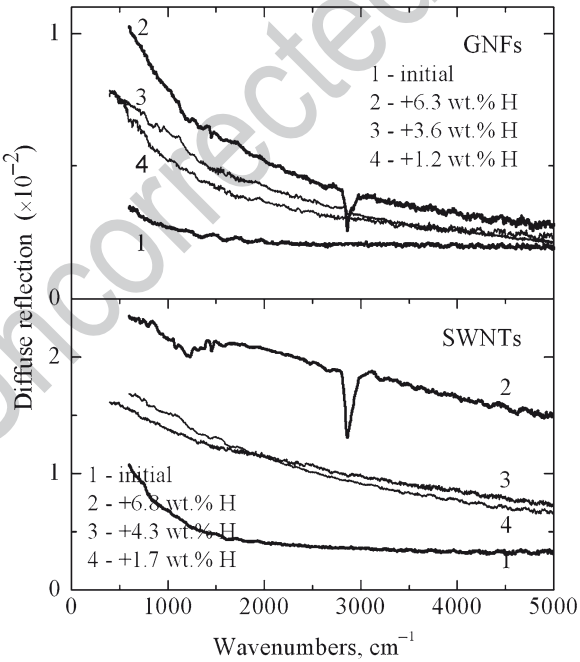

Fig. 11.5 IR diffuse reflection spectra of graphite nanofibers and single-walled carbon nanotubes: in the initial state, after saturation with hydrogen at 9 GPa, after removal of about 40% of absorbed hydrogen, and after degassing annealing. T = 300 K

BookID 185609_ChapID 11_Proof# 1 - 27/01/2010

After hydrogenation, the GNF diffused reflection increases substantially over the entire range of measurements (curves 2 of Fig. 11.5) and a narrow absorption band at 2,860 cm^{-1} with a halfwidth of 38 cm^{-1} and a weaker band at 2,920 cm^{-1} appear in the spectrum. These energies are typical of the stretching C–H vibrations, which are strong chemical bonds. In the spectra of hydrogenated SWNTs, the diffused reflection also increases; an asymmetric band with a maximum at 2,860 cm^{-1} and a halfwidth of 95 cm^{-1} appears in the spectrum due to the stretching C–H vibrations, as well. The asymmetry of the SWNT–H_x line can be explained by the overlap between the bands at 2,860 and 2,920 cm^{-1}.

After annealed for 6 h in vacuum at 700°C and removal of the main hydrogen mass, the C–H absorption lines disappear and the spectra become somewhat closer to the spectra of initial samples (curves 4 on Fig. 11.5). Nevertheless, the background diffuse reflection is regained in part and occupies the intermediate position between the spectra of the initial and hydrogenated samples.

Diffused reflection from powder sample is a complex combination of transmission, internal and external reflections, and scattering. It is dependent on the particle size, absorption and refractive indices of the studied material. The case of proper prepared powder diffuse reflection R carries the information primarily about the transmission spectrum of the sample (Willey 1976; Fuller and Griffiths 1978). The traditional method of the absorption spectra (K) calculation on the base of the diffused reflection R is the Kubelka–Munk equation $K = (1 - R)^2S/2Rc$, where S is the scattering coefficient, concentration of the studied material is c = 1 in our case.

[AU7]

Is it a real absorption? It is well known that analysis on the base of the Kubelka–Munk equation is applicable at diffuse reflection R not much less than $R \approx 30\%$. The case of low diffuse reflection the deviations from linearity should be taken into account. We have R is near 1%. So, we should be careful! The case of strongly absorbing samples it is possible to dilute them in nonabsorbent powder, for example in KBr powder. We have not used this traditional method because were afraid of possible chemical reactions at nigh temperature treatment of the mixture of the hydrogenated SWNTs with KBr.

We have elucidated the problem of the low diffuse reflection in (Bazhenov et al. 2004). Our hydrogenated carbon nanostructures are bulk polycrystalline materials. They are not responsible for IR measurements. We cleaved polycrystalline samples into thin plates and compare their optical properties with grinded samples. Absorption lines associated with vibration modes of the C–H bonds were well detected in the transmittance spectrum of $C_{60}H_{36}$ plates with the help of IR microscope of the Fourier spectrometer. This method was not applicable, however, for the study of SWNTs and NFs due to the strong free carrier absorption and variation of the plate thickness. The grinding of $C_{60}H_{36}$ does not result in a loss of the strongly bonded hydrogen (≈2,900 cm^{-1}). We are shure that grinding is applicable for strongly bonded hydrogen both for NFs and SWNTs as well.

To understand, are the spectra of Fig. 11.6 real absorption or not, we have studied the transmission spectra of the SWNT powder pressed in KBr pellets (Bazhenov

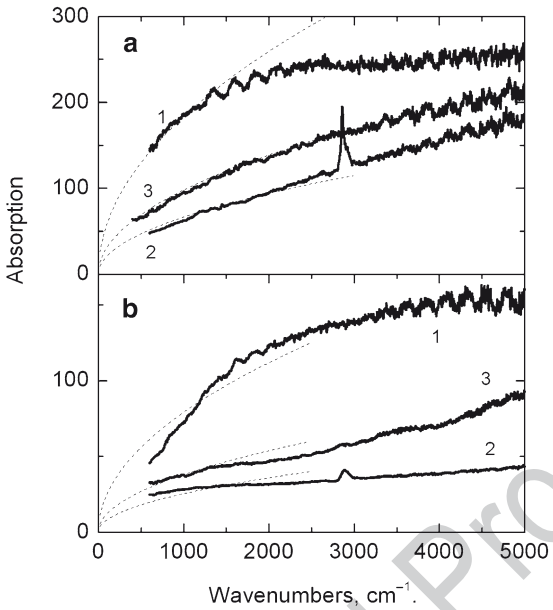

Fig. 11.6 Absorption spectra K restored from diffusive reflection R by using the Kubelka–Munk equation. Spectra 1, 2, and 3 are initial nanostructures, hydrogenated and annealed at 700°C during 6 h, respectively. (**a**) Spectra of NFs, (**b**) SWNTs. Dashed curves are Drude approximation of the absorption spectra, $K = A_i * \nu^{0.5}$

et al. 2004). For both cases we have used analysis on the base of Druder approximation of the free carrier conductivity in the spectral range $\nu < 1{,}500$ cm^{-1}. Using Drude formulas for high-frequency conductivity of the free carries we have got an absorption coefficient K of the free carries $K^2 = 16\pi^2\sigma\nu/c$ at low wave numbers ν, $\nu \ll \gamma$, where γ is the damping factor of free carriers, σ – high-frequency conductivity, c – velocity of light. These dependencies are shown in Fig. 11.6 by dashed curves. They have shown the ten times decrease of the free carrier absorption and, respectively, high-frequency conductivity of the free carries as a result of hydrogenation of SWNTs in both cases. So, we have qualitative concurrence of the results of these two methods.

At $\nu > 2{,}000$ cm^{-1} spectral dependence of monotonies increase of the absorption calculated from our diffuse reflection spectra is strongly different of the absorption spectra of SWNT powder pressed in KBr pellets. This is a result of strong absorption of light by SWNT nanoclusters. To study spectra in this spectral range we have used more complicate method: we have prepared SWNT thin films (Bazhenov et al. 2006). It was not an easy procedure, because it is well known that common organic solvents are not applicable in the case of carbon nanotubes. By date, there are no methods of synthesis of individual nanotubes of certain type. Nanotubes are generally combined into either ropes with hexagonal packing (bundles). This circumstance impedes their practical use. Grinding or treating samples with ultrasound in

BookID 185609_ChapID 11_Proof# 1 - 27/01/2010

an organic solvent (acetone, toluene) or an aqueous solution of a surfactant, can give a liquid suspension of nanotubes. However, such a suspension is unstable in time due to the van der Waals interaction between nanotubes. It leads to aggregation of nanotubes and precipitation of aggregates.

To prepare thin films of hydrogenated SWNTs we have dispersed them in acetone by a 10-min ultrasonic treatment. The prepared suspension was then dropped on a CaF_2 or KBr substrates and dried (Bazhenov et al. 2006). Suspension and drying at room temperature resulted in inhomogeneous distribution of nanotubes, because SWNTs got significantly aggregated while drying. The rate of aggregation increased by an order of magnitude for the hydrogenated SWNTs. To get homogeneous films, the suspension was pulverized on the substrates heated to ≈100°C. The preheating efficiently suppressed aggregation of both initial and hydrogenated SWNTs. Films of the initial SWNTs thus prepared were free of acetone, whereas some amount of this solvent (presumably, physisorbed) still remained in the films of the hydrogenated SWNTs To remove acetone, films of the hydrogenated SWNTs were heated to 150°C in vacuum.

The optical density spectra of thin films (Fig. 11.7) of the initial and hydrogenated SWNTs (5.4 wt% H) show a monotonic increase in the absorption with increasing photon energy in the spectral range 400–4,000 cm^{-1}. Taking into account that our samples are a mixture of metallic and semi conducting SWNTs (Mintwire et al.

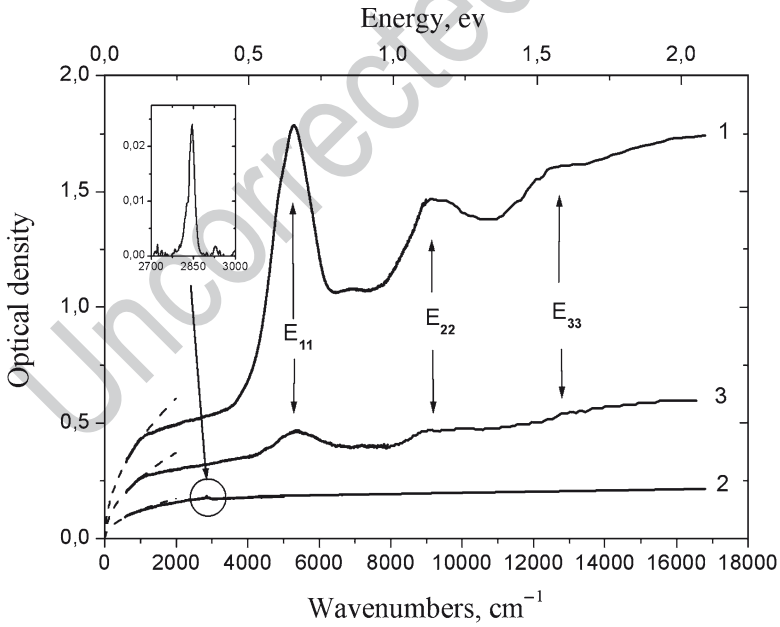

Fig. 11.7 Optical density spectra of thin films of the initial hydrogenated and outgassed SWNTs (spectra 1, 2 and 3, respectively). The dashed curves in the low-energy part of the spectra represent the Drude approximation of the absorption spectra. The inset in Fig. 11.7 shows the absorption lines of the C–H bonds in a thin film of the hydrogenated SWNTs

1992; Hamada et al. 1992; Saito et al. 1992), this increase of absorption is caused by high-frequency conductivity of the free carriers in metallic nanotubes. Relative intensities of the spectra of Fig. 11.7 we have found as a result of the diffuse reflection measurements of powders at low wavenumbers. The discussed above Drude approximations of the low-energy part of the absorption spectra are shown by dashed curves in gives Fig. 11.7. Comparison of the spectra 1 and 2 shows that hydrogenation decreases high-frequency conductivity of the SWNTs by one order of magnitude.

Optical density spectra of thin films of the initial SWNTs also demonstrate distinct absorption peaks at 0.62, 1.13 and 1.65 eV (spectrum 1 of Fig. 11.7). These absorption lines result from the van Hove singularities in the density of electron states due to the one-dimensional nature of nanotubes (Lin and Shung 1994). [AU8]

The first two lines are the transitions in the semiconducting SWNTs, the third line is the transition in the metallic SWNTs (Chiang et al. 2001). The spectral position of E_{11} = 0.62 eV of the first peak permits evaluating of the average diameter d of the semiconducting SWNTs as $d = 2a\delta/E_{11}$ = 1.2 nm in good agreement with the value 1.5 nm derived from the electron-microscopy data.

Peaks E_{11}, E_{22} and E_{33} disappear after hydrogenation (Fig. 11.7, spectrum 2) and a new narrow line arises at 2,845 cm^{-1} (0.353 eV), inset of Fig. 11.7. This line indicates the formation of the strong covalent C–H bonds in the samples as in the diffuse reflection spectra (Figs. 11.5 and 11.6). Study of the thin films has shown a liner dependence of the C–H peak intensity as a function of the hydrogen content. Such proportionality have shown that the most amounts of H atoms were covalently bonded to carbon atoms. The intensity of the line 2,845 cm^{-1} calculated from the diffuse reflection steeply decreases on outgassing and significantly deviates from the linear dependence. This discrepancy can be explained assuming that powder particles in the partly outgassed SWNTs were inhomogeneous: their outer layers were depleted in hydrogen. In fact, diffuse reflection can only feel a very thin surface layer of the particles due to the large value of the free carrier absorption coefficient $K \cong 10^4$ cm^{-1} for SWNTs, while the measured hydrogen content is related to the mean hydrogen content in the material.

The term “covalent” we should use carefully. It is perfect for the Si- or Ge-single crystals. In our case of carbon nanotubes with H we should take into account the transfer of electron between hydrogen and carbon cage, inevitably. So, some iconicity we should take into account. The transfer of electron between hydrogen and carbon cage may explain the disappearance of the E_{11}, E_{22} and E_{33} peaks as a result of hydrogenation of the SWNTs. Transfer of electrons between carbon cage and hydrogen will change the filling of the van Hove singularities (Fig. 11.8). It can explain the observed disappearance of the electronic transitions in the spectra of hydrogenated SWNTs.

The decrease of the free-carrier absorption upon hydrogenation can be associated with localization of free carries near C–H bonds in SWNTs, or increase in the rate of their scattering by these defects. The complete removal of hydrogen by vacuum annealing at 700°C only partly restored the intensity of the

BookID 185609_ChapID 11_Proof# 1 - 27/01/2010

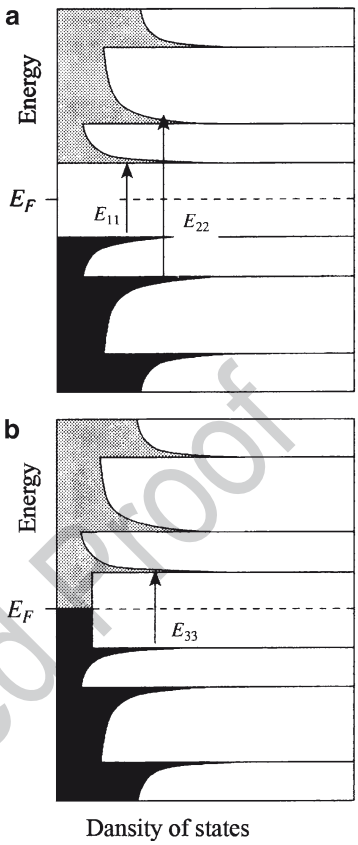

Fig. 11.8 Sketch of the energy structura and IR-active optical transitions E_{ii} in semiconducting (**a**) and metallic (**b**) SWNTs. Painted on the base of the theoretical calculations (Lin and Shung 1994; Chiang et al. 2001)

[AU9]

electronic transitions and free carrier absorption characteristic of the initial SWNTs. We think, some defects appear in the structure of SWNTs as a result of their hydrogenation at high pressure and removal of hydrogen. We have made a control experiment: SWNTs were exposed to the same power-temperature conditions but without hydrogen. This experiment has shown that electronic transitions vanish in the IR transmission spectrum and free carrier absorption strongly decreases as well. No doubt, mechanical interaction between SWNTs is different of the case of hydrogenation. It follows from the restoration (not complete) of the electron transitions and free-carrier absorption in SWNTs after degassing. Nevertheless, this control experiment permits to suppose the formation of some defects in the structure of SWNTs as a result of high-pressure hydrogenation.

Micro-Raman spectroscopy of the SWNTs hydrogenated at P = 5.0 GPa and T ≅ 500°C have shown a giant structureless hot luminescence background that screens all vibration modes (Meletov et al. 2007). Among them, the most interesting

for our study ware those with frequencies close to the Raman frequencies of the C–H stretching vibrations of the covalently bonded hydrogen (2,800–3,000 cm^{-1}) and of the H–H stretching vibration of the molecules H_2 (4,130–4,160 cm^{-1}). But, we could not detect them at excitation of the Raman spectra with the help of Ar^+, or Kr^+ lasers. The intensity of the luminescence background is about a 100 times stronger than that for pristine SWNTs. High intensity and frequency dependence of this luminescence are typical for hot luminescence: intensity of the spectrum and frequency dependence have no changed when we have used 488 and 514.5 nm line of an Ar^+ laser, as well as the 647.1 nm line of a Kr^+ laser for excitation. Hot luminescence was attributed to the random binding of the hydrogen atoms on the surface of SWNTs. Hot luminescence vanishes after annealing of the hydrogenated SWNTs in vacuum or in air.

Besides, we have measured Raman spectra of the SWNTs treated under the same high pressure and temperature (HPHT) conditions as those used for the hydrogenation of SWNTs (P = 5.0 GPa, T = 500°C) but without hydrogen atmosphere (spectrum (b) of Fig. 11.9) and spectrum of the hydrogenated SWNTs after their complete degassing at 500°C in vacuum (spectrum (c) of Fig. 11.9). The spectra (b) and (c) were compared with the spectrum (a) of the pristine SWNTs. Note that, the luminescence background in spectrum (b) of the HPHT treated SWNTs is not as high as in the spectra of hydrogenated SWNTs. The main difference between the spectra (a), and (b), (c) is in the broadening of all the Raman peaks in comparison with the spectrum of pristine SWNTs (spectrum (a)), the increase of the D-band intensity, and the appearance of the second-order $D+G^+$ peak at 2,945 cm^{-1}. Raman spectra of pristine SWNTs had shown narrow peaks and a very small intensity of the

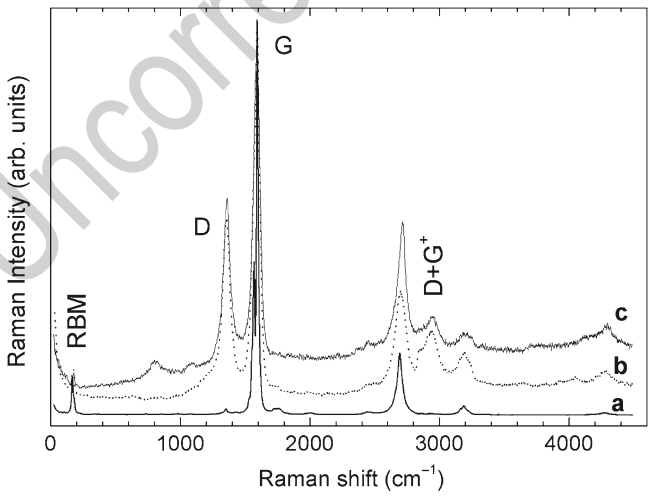

Fig. 11.9 Raman spectra of (**a**) pristine SWNTs (**a**), (**b**) SWNTs treated at high pressure and high temperature in the absence of a hydrogen atmosphere, and (**c**) hydrogenated SWNTs after annealing in vacuum at ≅550°C for 1 h

D-band at 1,350 cm^{-1} typical for SWNTs of the high structural order. It is known that the D-band in graphite-related materials is associated with structural disorder while a double-resonance process was employed for their interpretation (Thomsen and Reich 2000). The intense Raman G-band at a higher energy corresponds to the C–C stretching vibrations in tangential and axial directions of the SWNT that splits to G^- (tangential) and G^+ (axial) bands located at 1,567 and 1,592 cm^{-1}, respectively. The shape of the G^--band is sensitive to the electronic properties, strongly related to the diameter and chirality of SWNTs: the Lorentzian lineshape is characteristic of the semiconducting SWNTs, whereas the Breit-Wigner Fano lineshape is typical for metallic SWNTs (Venkateswaran 2004). In our case, the Lorentzian lineshape of the G^--band indicates that the probed SWNTs are semiconducting. The low-frequency Raman band is related to the radial breathing modes (RBM) of the tubes. Its spectral position is using for calculation of the diameter of carbon nanotubes.

Taking into account the results of the IR and Raman scattering measurements, we may conclude that not complete restoration of the IR spectra after outgassing of the hydrogenated SWNTs is a result of appearance of structural disorder in SWNTs due to high pressure/high temperature hydrogenation.

11.3 High-Pressure Hydrogenated C_{60}

As we told above, there were prepared compounds $C_{60}H_x$ and $C_{70}H_x$ with even values of x by chemical reaction of hydrogen with C_{60}. The most complete study of their properties was carried out on $C_{60}H_{36}$ and $C_{60}H_{18}$ and discussed in many reviews (e.g. Taylor and Walton 1993; Hirsch 1994; Goldshleger 1997).

Maximal content of hydrogen was x = 36.

Hear we want to discuss properties of the $C_{60}H_{36}$ prepared by high-pressure technic. The $C_{60}H_{36}$ molecule may exist in a great number of isomeric forms, but only a small number of them are stable (Bühl et al. 1995). The isomeric form with the highest symmetry, T_h, has 12 double bonds, arranged as far apart as possible on the surface of the C_{60} cage, while the form having the double bonds in four isolated aromatic six-membered rings lacking hydrogen atoms and located at the corners of a tetrahedron has a T symmetry structure. Between these two extremes are the isomers with symmetry D_{3d} and S_6, which have two six membered rings at the three-fold axis poles of the molecule, with the other six double bonds isolated in six pentagons. The presence of various isomers in the $C_{60}H_{36}$ specimens depends most likely on the preparation method and on the kinetic parameters controlling hydrogen addition. For example, $C_{60}H_{36}$ prepared by hydrogen transfer from a hydrogen-rich compound like 9,10-dihydroanthracene contains a mixture of the principal isomers D_{3d} and S_6, while $C_{60}H_{36}$, prepared by zinc reduction of C_{60} in aromatic solvents, contains the S_6 isomer as the most abundant (Bini et al. 1998; Bensasson et al. 1997; Darwish et al.1995).

Concerning the solid-state phase of $C_{60}H_{36}$, Hall et al (1993) have suggested the body-centered cubic structure (bcc) with cell parameter 11.785 ± 0.015 Å for the

packing of the molecules in the crystalline state. Furthermore, they suppose, at least for the D_{3d} isomer, that at low temperatures the **bcc** crystal structure would be transformed to a body-centered tetragonal one.

The connection of the 36 hydrogen atoms to the C_{60} cage lowers the molecular symmetry and activates Raman scattering from a variety of initially forbidden phonon modes (Bini et al. 1998). In addition, the appearance of the C–H stretching and bending modes and those related to various isomers of $C_{60}H_{36}$, results in a very rich Raman spectrum. The comparison of the phonon frequencies for five principal isomers of $C_{60}H_{36}$, obtained by molecular dynamics calculations, with experimentally observed phonon frequencies has led to the conclusion that the material prepared by the transfer hydrogenation method contains mainly two isomers, those with symmetries D_{3d} and S_6 (Bini et al. 1998).

In revue (Meletov and Kourouklis 2005) we have analyzed optical Raman and photoluminescence spectra of the hydro- and deuterofullerene, $C_{60}H_{36}$ and $C_{60}D_{36}$, respectively, prepared by high-pressure hydrogenation. The X-ray analysis, of the obtained material, shows that it has the **bcc** structure, typical for $C_{60}H_{36}$ (Hall et al. 1993), with lattice parameter 11.83 Å. The aim of research was to identify the phonon and electron energy spectra of the high-pressure hydrogenated fullerene, to clarify the isomer composition and homogeneity of samples, as well as to study the isotopic effects in the vibrational spectra. The Raman spectra of the high-pressure hydrogenated samples were compared with those obtained by transfer hydrogenation and with the molecular dynamics calculations data, five low energy isomers were studied (Bini et al. 1998). The Raman data show the presence of all principal isomers in the high-pressure hydrogenated fullerenes, large isotopic shift for the C–H stretching mode, whereas the shift of the modes related to the fullerene molecular cage is negligible. We have also studied the pressure behavior of the Raman and photoluminescence spectra of the $C_{60}H_{36}$ at pressure up to 12 GPa in order to get information about the structural and chemical stability of the material at high pressure. All observed features are reversible with pressure and $C_{60}H_{36}$ is stable in the investigated pressure region. [AU12]

The comparison of our experimental data with those of Ref. (Bini et al. 1998; Bensasson et al. 1997) shows that the Raman spectrum of the high-pressure hydrogenated $C_{60}H_{36}$ is richer more than five times than that of the transfer hydrogenated $C_{60}H_{36}$. The majority of the experimentally observed Raman peaks (86 peaks from a total number of 126) are very close, with an accuracy of ~5 cm^{-1}, to the calculated frequencies and cross-sections of the Raman active modes (their total number is 400) (Bini et al. 1998). The peaks, which are close to the calculated frequencies, are assigned to all principal isomers, but the majority of them belong to the isomers with the symmetry S_6, T and D_{3d}.

Now we want to discuss IR optical spectra of the $C_{60}H_{36}$ synthesized at high-pressure. Results of this study were published in Bazhenov et al. (2008). There are a lot of publications devoted to theoretical and experimental study of $C_{60}H_{36}$. We should pay attention on the existing discrepancies in the results of theoretical calculations of the dipole-active spectra $C_{60}H_{36}$, compare, for example, papers Bini et al. (1998) and Bulusheva et al. (2001). There were used different theoretical models. Semiempirical method of the MNDO type (Dewar and Thiel 1977) was used in (Bini et al. 1998). Ab initio Hartree–Fock self-consistent field approximation was used in (Bulusheva et al. 2001). [AU13]

To analyze structure of $C_{60}H_{36}$ produced by our method we elucidated absorption spectra near 2,900 and 1,650 cm^{-1}. It was found that Lorenz curves are the best approximations of the spectra determined by the stretching vibrations of the C–H bonds in $C_{60}H_{36}$. Figure 11.10 shows that the structure of stretching vibrations strongly depends on hydrogen content x. Experimental spectrum of stretching vibrations in $C_{60}H_{48}$ consists of two broad lines 2,914 and 2,841 cm^{-1} and of four lines 2,912, 2,860, 2,830, 2,802 cm^{-1} in $C_{60}H_{36}$. We denote these lines in $C_{60}H_{36}$ as 1, 2, 3 and 4, respectively. The order of their relative intensities is $1 > 2 > 3 > 4$. Infrared and Raman spectra of five low energy isomers of $C_{60}H_{36}$ of the T_h, D_{3d}, D_{3d}(C-K), T and S_6 symmetries were simulated in (Bini et al. 1998) by semiempirical quantum chemical calculations. In accordance with (Bini et al. 1998) the main part of our $C_{60}H_{36}$ is close to the T symmetry. Two discrepancies with experiment we have found: (1) experimental and theoretical intensity orders are $1 > 2 > 3$ and $1 > 2 \gg 3$, respectively; (2) experimental and theoretical intervals of three high energy lines are 82 and 39 cm^{-1} (for T symmetry), respectively. Essentially more close to our experimental frequencies and intensity order were calculated for $C_{60}H_{36}$ of T symmetry using ab initio Hartree–Fock self-consistent field (Bulusheva et al. 2001). Tree high energy lines in our high-pressure hydrogenated $C_{60}H_{36}$: 2,912, 2,860, 2,830 cm^{-1} in $C_{60}H_{36}$ and their relative intensities are close to the $C_{60}H_{36}$ of the T symmetry 2,912, 2,850, 2,831 cm^{-1} in the chemically synthesized $C_{60}H_{36}$ (Bulusheva et al. 2001).

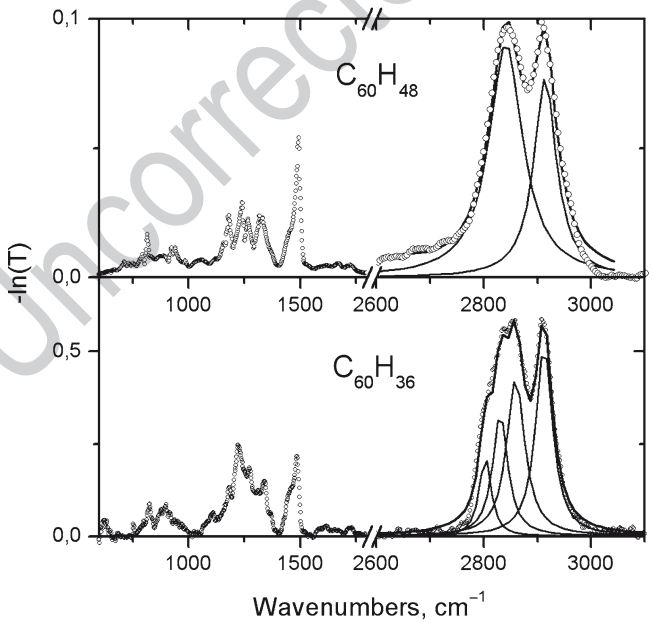

Fig. 11.10 Absorption spectra of $C_{60}H_{36}$, $C_{60}H_{48}$ and their deconvolution: points are experimental spectra; thin solid lines designate the Lorenzian curves and the sum of these curves

In accordance with (Bini et al. 1998) absorption line 4 in $C_{60}H_{36}$ may be explained by admixture of the isomer of the D_{3d} symmetry. Absorption spectrum of $C_{60}H_{36}$ near 1,650 cm^{-1} confirms an admixture of isomers in our case. Theoretical calculations (Bini et al. 1998) have shown absorption lines at 1,634, 1,700 and 1,731 cm^{-1} in isomers of D_{3d}, T_h, D_{3d}(C-K) symmetries, respectively, and absence of absorption in this spectral range in isomers of S_6 and T symmetries. But T-isomer should have absorption line near 1,700 cm^{-1} in accordance with calculations (Bulusheva et al. 2001). We have observed absorption lines at 1,584, 1,611 and 1,723 cm^{-1}. It means that we have not only admixture of the isomer of the D_{3d} symmetry, but isomer of the D_{3d}(C-K) or T_h symmetry as well.

So, we may conclude that we have combination of isomers in our $C_{60}H_{36}$ synthesized at high-pressure and high temperature in accordance with IR and Raman measurements.

Authors of the course of fullerene chemistry (Fullerenes, Ed. "Examen" 2005) are sure that carbon cage of the hydrogenated fullerene with $x > 36$ should be destroyed as a result of steric strains. Experiment (Talyzin et al. 2006) has shown that increase of [AU14] the hydrogenation time at hydrogen pressure 120 bar and temperature T = 673 K results in amorphization of the structure at hydrogen content more than 4.6 wt% (formally $x \geq 36$). The sample with the strongest hydrogenation (5.3 wt%) was completely amorphous. Nevertheless, high-resolution mass spectroscopy of these samples has shown some amount of highly reduced fullerenes up to $C_{60}H_{50}$ and fragments of $C_{57-59}H_x$ with variation of the hydrogen content x from 38 to 48 (Talyzin et al.(2006). The change of the conditions of hydrogenation (20 kbar, T = 773 K, 90 min) has shown that it is possible to produce hydrofullerides $C_{60}H_x$ with $44 \leq x \leq 52$ without noticeable fragmentation or collapse of the carbon cage (Talyzin et al. 2006). It is important that in the case of high pressure of hydrogenation mass spectroscopy has shown essentially more narrow $C_{60}H_x$ distribution, $44 \leq x \leq 52$ (Talyzin et al. 2006), in comparison with the hydrogenation at low pressure ($16 \leq x \leq 50$) (Talyzin et al. 2006). The resultant product is strongly dependent on the experimental method of hydrogenation of C_{60}, and further study of the strongly reduced fullerenes is necessary.

Our method of high-pressure/high temperature is essentially different of the chemical methods of hydrogenation of C_{60}. We have synthesized $C_{60}H_x$ with $36 \leq x \leq 60$ at hydrogen pressure 50 ± 5 kbar, temperatures up to 773 K and time of hydrogenation ≅10 h. Hydrogenated samples were of white color. The value of hydrogen content x was dependent on the experimental conditions: time, temperature, pressure. Hydrogen content in products was estimated by combustion of fulleranes in the oxygen flow and weighting of the resultant products, CO_2 and H_2O. Average hydrogen content was measured in our case with accuracy $\Delta x = \pm(0.5 \div 1)$. We do not know the exact formula for every C_{60} molecule in the product of hydrogenation: the case of one experiment we have got x = 57.5, second experiment has shown x = 60.1. We think that we have $C_{60}H_{60}$ molecules with some admixture of impurity.

IR transmission spectra (T) of the thin polycrystalline specimens or powders were measured using IR microscope of the Fourier-spectrometer at room temperature in the spectral range of 600 ÷ 5,000 cm^{-1}. Optical absorption spectra were calculated as −ln(T). Figure 11.11 demonstrates normalized absorption spectra of fulleranes $C_{60}H_x$ with x = 36, 42, 48 and 60 together with the well known spectrum of fullerit

BookID 185609_ChapID 11_Proof# 1 - 27/01/2010

C_{60} (bottom picture). Stretching and banding vibrations of the C–H bonds appear in the spectra of the hydrogenated C_{60} near 2,900 and 1,450 cm^{-1}, respectively. Also, the well-known increase of a number of dipole-active modes determined by vibrations of the carbon cage was observed when we got over from highly-symmetrical C_{60} to fulleranes $C_{60}H_x$ with x = 36, 42, 48. This is a result of the lowered molecular symmetry and existence of isomers. For example, fullerit C_{60} has 4 dipole-active modes; $C_{60}H_{36}$ of the T symmetry should have 42 dipole-active modes in accordance with theoretical calculation (Bini et al. 1998). A number of the dipole-active vibration modes decreased again in $C_{60}H_{60}$. This indicates their higher symmetry in comparison with $C_{60}H_x$, x = 36 ÷ 48. Our IR spectrum of $C_{60}H_{60}$ is similar to that one measured in highly reduced fullerit with x = 44 ÷ 52 (Talyzin et al. 2006). Taking into account results of paper (Talyzin et al. 2006). it is possible to conclude that carbon cage of C_{60} is not destroyed in our $C_{60}H_{60}$.

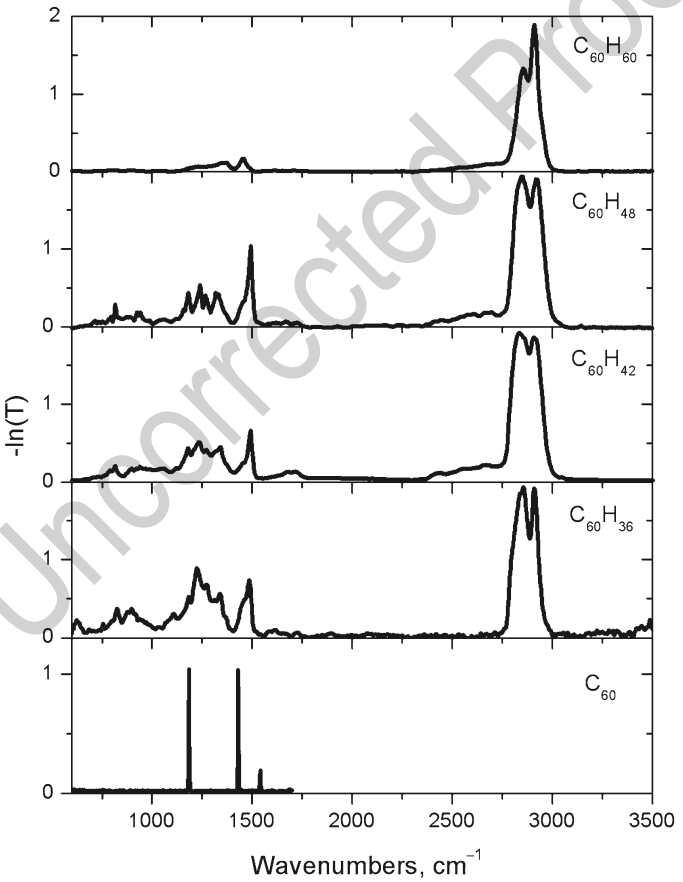

Fig. 11.11 Normalized absorption spectra of fullerit C_{60} and fulleranes $C_{60}H_x$ with x = 36, 42, 48 and 60, T = 300 K

It is interesting that a combination of the vibrational modes of $C_{60}H_{60}$ and, for example, $C_{60}H_{48}$ may explain the emission and absorption spectra of interstellar and circumstellar clouds. Millimitre-wave measurements have led to the detection of over 120 inorganic, organic molecules, radicals, cyclic molecules, and cyanopoynes in the interstellar medium (Kwok 2004). In addition to molecules, solid-state particles were found in the interstellar and circumstellar medium. Solid particles have a high opacity due to strong absorption and scattering of the visible light. These clouds of dust may completely obscure the stars. Clouds may be studied by infrared absorption spectroscopy as well. Infrared emission spectrum of the carbon-rich source NGC 7027 (Russel et al. 1977). is shown in the upper part of Fig. 11.12.

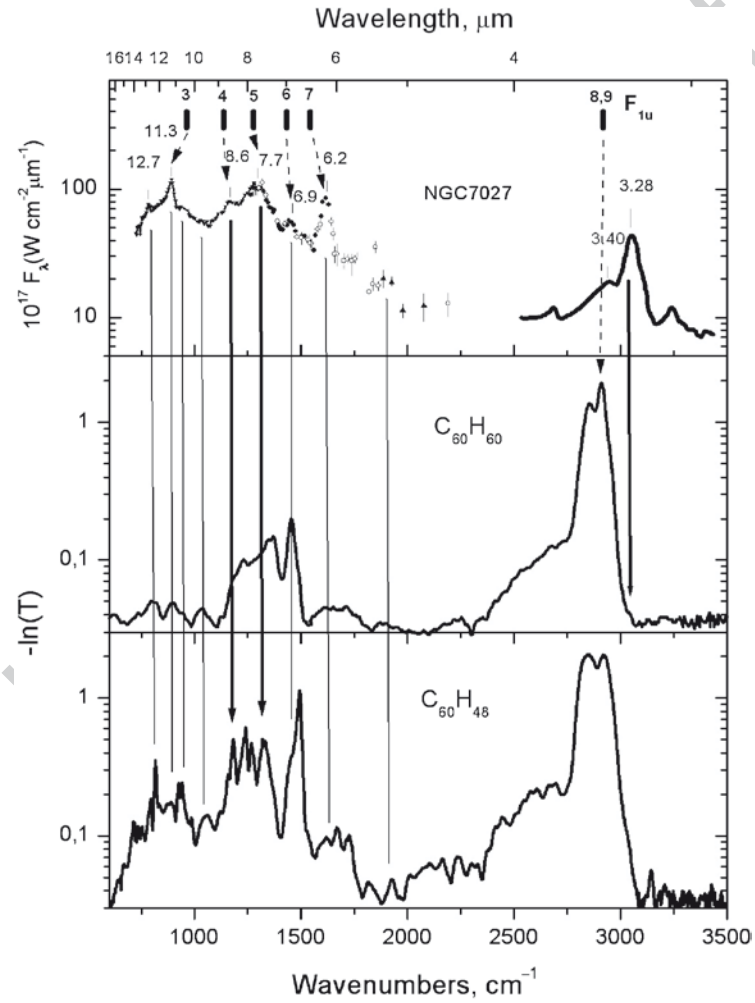

Fig. 11.12 Emission spectrum of NGC 7027 with the wavelengths of the unidentifined features marked and normalized absorption spectra of $C_{60}H_{60}$ and $C_{60}H_{48}$

BookID 185609_ChapID 11_Proof# 1 - 27/01/2010

This emission is a result of illumination of the interstellar and circumstellar clouds excited by ultraviolet radiation of stars. A lot of experiments were performed in different laboratories to fit the C–H starching features observed towards the Galactic center: complex molecular mixture formed by irradiation of ices, hydrogenated amorphous carbon, quenched carbonaceous composite produced by quenching the plasma of methane gas, organic materials, such as microorganisms (see references in (Pendelton et al. 1994)). None of widely accepted materials were satisfactory for explanation of the emission spectrum of NGC 7027 (Webster 1991). Adrian Webster (Webster 1991, 1993) proposed that this spectrum is the emission of $C_{60}H_{60}$ and $C_{60}H_x$ with small x. He has calculated vibrational spectrum of $C_{60}H_{60}$, using a force-field model. He has supposed that carbon atoms in $C_{60}H_{60}$ are located at the vertices of a truncated icosahedron as in usual C_{60}, and the bound hydrogen atoms positioned randomly outward from them (I_h symmetry, the icosahedral grope with inversion). Of the possible 354 vibrational modes in $C_{60}H_{60}$, only 27 belonging to the irreducible representation F_{1u} are IF-active. This representation is triply degenerate, so there are nine IR active frequencies. The result of theoretical calculation is shown by short vertical lines in the upper part of Fig. 11.12. Tentative assignment of calculated frequencies of $C_{60}H_{60}$ to unidentified infrared features is shown by arrows in this figure. Six of the infrared active frequencies match unidentified lines to within 4%, and a seventh differ from an observed line by 8%. Line 787 cm^{-1} (12.7 μm) was not identified. Experimental spectrum of $C_{60}H_{60}$ much better describes unidentified lines. Moreover, not identified in theory (Webster 1991, 1993) line 787 cm^{-1} (12.7 μm) is clearly seen in experimental spectrum.

Two features of the unidentified emission cannot be explained with the help of theoretical and experimental spectra of $C_{60}H_{60}$: broad backgrounds in the spectral range 700 ÷ 1,700 cm^{-1}, and emission line at 3049 cm^{-1} (3.28 μm). It was supposed in (Webster 1991, 1993) that background is an emission of lightly hydrogenated fulleranes $C_{60}H_x$ as a result of decreased molecular symmetry and isomerism. As an example we show spectrum of $C_{60}H_{48}$ in Fig. 11.12. Strong background in the spectral range 700 ÷ 1,700 cm^{-1} takes place in this spectrum. As we have shown above, our fulleranes with hydrogen content x = 36 are a mixture of isomers. We are sure that the same will take place at x = 48. Figure 11.10 shows an increase of background in the spectrum of $C_{60}H_{48}$ in comparison with the spectrum of $C_{60}H_{36}$.

Cataldo F. (2003) the first have shown that the absorption spectrum of $C_{60}H_{36}$ synthesized by chemical method is able to match several IR emission lines detected from interstellar carbon dust. Background in the spectral range 700 ÷ 1,700 cm^{-1} was not detected in this paper.

Stretching vibrations of C–H bonds in experimental absorption spectrum near 1,920 cm^{-1} correspond to the sp^3 bonding (Stoldt et al. 2001) (Fig. 11.3). They are observed in emission spectrum of NGC 7027 as a broad band overlapping with line 3,049 cm^{-1} (3.28 μm). This line was never observed in absorption spectra of interstellar and circumstellar clouds (Russel et al. 1977). Frequency of this line corresponds to the sp^2 bonding (Stoldt et al. 2001). We should note that vary weak line 3,050 cm^{-1} was observed in the absorption spectra of synthesized $C_{60}H_{42}$ and $C_{60}H_{60}$ (Fig. 11.13). Taking into account strong steric strains in highly reduced

fulleranes, we suppose that a high concentration of short time leaving sp^2 bonds appear in $C_{60}H_x$ with $x \geq 42$ at ultraviolet excitation by stars. The absence of this line in the absorption spectra of interstellar and circumstellar clouds may be explained by emission of only thin boundary layer of cloud as a result of absorption of the ultraviolet light of stars by dust of cloud and shot lifetime of the sp^2 states.

The absorption spectrum of stretching vibrations of the C–H bonds consists of three lines 2,857, 2,910 and 2,942 cm^{-1} (Fig. 11.13). Analogous structure is seen in the absorption spectrum of the cloud IRS6E (Fig. 11.13).

Fig. 11.12 shows that the emission intensity of the low energy states is stronger than that of the high energy lines. The absorption spectra of Fig. 11.12 have reverse relation. Absorption is proportional to the density of the vibrational states. Emission intensity is proportional to the Boltzmann population of the vibrational states at ultraviolet excitation. This may be a reason for high emission intensity of the low energy states in clouds.

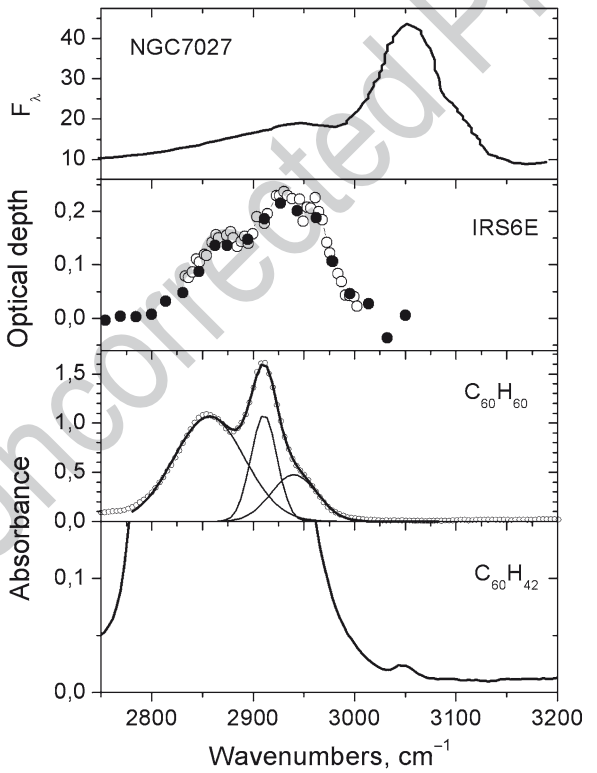

Fig. 11.13 Emission spectrum of NGC 7027, absorption spectrum of the interstellar cloud IRS6E and absorption spectra of synthesized $C_{60}H_{60}$ and $C_{60}H_{42}$ in the range of the stretching vibrations of the C–H bonds

Acknowledgments This work was supported by the program of the Russian Academy of Sciences "Quantum Properties of the Condense Matter", by the Russian Foundation for Basic Research of the Russian Ministry of Science.

[AU15] ## References

Assink RA, Schirber JE, Loy DA, Morosin B, Carlson GA (1992) Mater J Res 7:2136

Bashkin IO, Antonov VE, Bazhenov AV, Bdikin IK, Borisenko DN, Krinichnaya EP, Moravsky AP, Harkunov AI, Shul'ga Yu M, Ossipyan Yu A, Ponyatovsky EG (2004) JETP Lett 79(5):226

Bazhenov AV, Kveder VV, Ossipyan YuA, Nikolaev RK, Fursova TN, Shalynin AI (1998) JETP 86(5):1030

Bazhenov AV, Fursova TN, Antonov VE, Bashkin IO, Harkunov AI, Ponyatovsky EG (2004) Fullerenes Nanot Carbon Nanostruct 12(1):293

Bazhenov AV, Fursova TN, Bashkin IO, Antonov VE, Kondrat'eva IV, Krestinin AV, Shulga YuM (2006) Fullerenes nanotubes and carbon nanostructures 14(2&3):165

Bazhenov AV, Fursova TN, Bashkin IO, Moravskii AP, Shulga YuM (September 2008) Fullerenes Nanot Carbon Nanostruct 16(5&6):579

Bensasson RV, Hill TJ, Land EJ, Leach S, McGarvey DJ, Truscott TG, Ebenhoch J, Gerst M, Rüchardt C (1997) Chem Phys 215:111

Bini R, Ebenhoch J, Fanti M, Fowler PW, Leach S, Orlandi G, Ruchardt C, Sandall JPB, Zerbetto F (1998) Chem Phys 232:75

Bühl M, Thiel W, Schneider U (1995) J Am Soc 117:4623

Bulusheva LD, Okotrub AV, Antich AV, Lobach ASJ (2001) Mol Struct 562:119

Cataldo F (2003) Fullerenes Nanot Carbon Nanostruct 11(4):295

[AU16] Chiang IW, Brinson BE, Huang AY, Willis PA, Bronikowski MJ, Margrave JL (2001a) J Phys Chem B 105:8297

Chiang IW, Brinson BE, Smalley RE, Margrave JL, Hauge RH (2001b) J Phys Chem B 105:1157

Darwish AD, Abdul-Sada AK, Langley GJ, Kroto HW, Taylor R, Walton DR (1995) J Chem Soc Perkin Trans 2:2359

Dewar MJS, Thiel WJ (1977) Am Chem Soc 99:4899

Dillon AC, Heben MJ (2001) Appl Phys A 72:133

Fuller MP, Griffiths PR (1978) Anal Chem 50:1906

Fullerenes, Ed. "Examen" (2005) Moscow, pp 245, 263, 285

Goldshleger NF, Moravskii AP (1997) Russ Chem Rev 66:323

Hall LE, McKenzie DR, Attalla MI, Vassallo AM, Davis RL, Dunlop JB, Cockayne DJH (1993) J Phys Chem 97:5741

Hamada N, Savada SI, Oshiyama A (1992) Phys Rev Lett 68:1579

Hirsch A (1994) Chemistry of fullerenes, Ch. 5. George Thieme Verlag, Stuttgart, p 117

Jin C, Hettich R, Compton R, Joyce D, Blencoe J, Burch TJ (1994) Phys Chem 98:4215

Krestinin AV, Raevskii AV, Kiselev NA, Zvereva GI, Zhigalina OM, Kolesova OI (2003a) Chem Phys Lett 381:529

Krestinin AV, Kiselev NA, Raevskii AV, Ryabenko AG, Zakharov DN, Zvereva GI (2003b) Eurasian Chem Tech J 5:7

Kwok S (2004) Nature 430:985

Lin MF, Shung KW-K (1994) Phys Rev B 50:17744

Loutfy RO, Lowe TP, Hutchison JL, Kiselev NA, Zakharov DN, Krinichnaya EP, Muradyan VE, Tarasov BP, Moravsky AP (1999) Abstracts of IV Workshop on Fullerenes and Atomic Clusters (IWFAC'99), St. Petersburg, 1999, pp. 117

751 Meletov KP, Kourouklis GA (2005) JETP 127:860
752 Meletov KP, Maksimov AA, Tartakovskii II, Bashkin IO, Shestakov VV, Krestinin AV, Shulga
753 YuM, Andrikopoulos KS, Arvanitidis J, Christofilos D, Kourouklis GA (2007) Chem Phys
754 Lett 433:335
755 Mintwire JM, Dunlap BI, White CT (1992) Phys Rev Lett 68:631
756 Pendelton YJ, Sandford SA, Allamandola LJ, Tielens AGGM, Seldgren LJ (1994) Astroph J
757 437:683
758 Pradhan BK, Sumanasekera GU, Adu CKW, Romero HE, Williams KA, Eklund PC (2002)
759 Physica B (Amsterdam) 323:115
760 Russel RW, Soifer BT, Merrill KM (1977) Astroph J 213:66
761 Saito R, Fujita F, Dresselhaus G, Dresselhaus MS (1992) Appl Phys Lett 60:2204
762 Sharma SM, Karmakar S, Sikka SK, Teredesai PV, Sood AK, Govindaraj A, Rao CNR (2001)
763 Phys Rev B 63:205417
764 Shigematsu K, Abe K, Mitani M, Tanaka K (1993) Chem Express 8:37
765 Shulga Yu M, Bashkin IO, Krestinin AV, Martynenko VM, Zvereva GI, Kondratieva IV, Ossipyan
766 Yu A, Ponyatovsky EG (2004) JETP Lett 80:752
767 Stoldt CR, Maboudian R, Carraro C (2001) Astroph J 548:L225
768 Talyzin AV, Tsybin YuO, Purcell JM, Schaub TM, Shulga YuM, Noreus D, Sato T, Dzwilewski A, [AU17]
769 Sundqvist B, Marshall AG (2006a) J Phys Chem A 110(27):8528
770 Talyzin AV, Dzwilewski A, Sundqvist B, Tsybin YuO, Purcell JM, Marshall AG, Shulga YuM,
771 McCammon C, Dubrovinsky L (2006b) Chem Phys 325(2):445
772 Taylor R, Walton DRM (1993) Nature 363:685
773 Thomsen C, Reich S (2000) Phys Rev Lett 85:5214
774 Venkateswaran UD (2004) Phys Stat Sol b 241:3345
775 Webster A (1991) Nature 352:412
776 Webster A (1993) Mon Not R Astron Soc 264:121
777 Willey RR (1976) Appl Spectrosc 30:593

Author Queries

Chapter No.: 11 0001142056

Queries	Details Required	Author's Response
AU1	Please provide e-mail id for the authors I.O. Bashkin and K.P. Meletov.	
AU2	The citation 'Taylor et al. 1993' (original) has been changed to 'Taylor and Walton, 1993' throughout. Please check if appropriate.	
AU3	'Goldshleger et al. 1997' is cited in text but not given in the reference list. Please provide details in the list or delete the citation from the text.	
AU4	"Krestinin et al. 2003; Krestinin. et al.2003" have been changed to "Krestinin et al. 2003a. b".	
AU5	Please specify the year "2003a" or "2003b".	
AU6	Please specify the year "2001a" or "2001b" throughout.	
AU7	The citation 'Fuller et al. 1978' (original) has been changed to 'Fuller and Griffiths, 1978'. Please check if appropriate.	
AU8	The citation 'Lin et al. 1994' (original) has been changed to 'Lin and Shung, 1994'. Please check if appropriate.	
AU9	The citation 'Lin et al. 1994' (original) has been changed to 'Lin and Shung, 1994'. Please check if appropriate.	
AU10	The citation 'Thomsen et al. 2000' (original) has been changed to 'Thomsen and Reich, 2000'. Please check if appropriate.	
AU11	'Goldshleger 1997' is cited in text but not given in the reference list. Please provide details in the list or delete the citation from the text.	
AU12	The citation 'Meletov et al. 2005' (original) has been changed to 'Meletov and Kourouklis, 2005'. Please check if appropriate.	
AU13	The citation 'Dewar et al. 1977' (original) has been changed to 'Dewar and Thiel, 1977'. Please check if appropriate.	
AU14	Please specify the year "2006a" or "2006b" throughout.	
AU15	The reference "Goldshleger and Moravskii 1997" is not cited in text. Please check.	
AU16	"Chiang et al. 2001" listed twice in the reference list has been changed to "Chiang et al. 2001a" and "Chiang et al. 2001b". Please update them in the text cross citations.	
AU17	"Talyzin et al. 2006" listed twice in the reference list has been changed to "Talyzin et al. 2006a" and "Talyzin et al. 2006b". Please update them in the text cross citations.	